Vol. 23, No. 1(2024) Poly24171
Revista Mexicana de Ingeniería Química

# Enhancing biocompatibility and antimicrobial efficacy through plasma technology modification of chitosan/*Rosmarinus officinalis* hydrogels

# Mejora de la biocompatibilidad y la eficacia antimicrobiana mediante la modificación con tecnología de plasma de hidrogeles de quitosano/*Rosmarinus officinalis*

C. G. Cuellar-Gaona[1], M.C. Ibarra-Alonso[2], R.I. Narro-Céspedes[3]*, M.G. Neira-Velázquez[1], M.D. Dávila-Medina[3], A. Zugasti-Cruz[3], S.C. Esparza-González[4], A. Sáenz-Galindo[3], E.O. Martínez-Ruiz[1]
[1]*Center for Research in Applied Chemistry, 25294 Saltillo, Mexico.*
[2]*CONACYT. Faculty of Chemical Sciences. Autonomous University of Coahuila, 25280 Saltillo, Mexico.*
[3]*Faculty of Chemical Sciences. Autonomous University of Coahuila, 25280 Saltillo, Mexico.*
[4]*Faculty of Dentistry. Autonomous University of Coahuila, 25125 Saltillo, México.*
Received: September 22, 2023; Accepted: December 13, 2023

## Abstract
The study of the modification of hydrogels by plasma technology is of great interest to the scientific community for its potential biomedical applications. This research aims to modify chitosan/*Rosmarinus officinalis* (*R. officinalis*) extract hydrogels to help convert it into a hydrogel with potential application as a wound dressing. Different chitosan/*R. officinalis* hydrogels, modified with plasma at 100, 150, and 200 W, were fabricated. Their biocompatibility properties and antimicrobial effect were evaluated, and they were characterized by Fourier-Transform Infrared Spectroscopy (FTIR), Thermogravimetric Analysis (TGA), Differential Scanning Calorimetry (DSC), and Scanning Electron Microscope (SEM), and evaluated for their degradability, swelling, and extract release. Plasma-modified hydrogels at 200 W obtained superior biocompatibility, presenting cell viability >80% and percentage of hemolysis <2%, for the evaluated concentrations of 1 and 2.5 mg/mL of the material, in turn, they presented greater antimicrobial effect against Staphylococcus aureus (*S. aureus*) and *Escherichia coli* (*E. coli*), compared to hydrogels modified at 100 and 150 W. At the same time, a higher percentage of *R. officinalis* extract release was obtained in the hydrogels with plasma treatment of 200 W, achieving a sustained release for up to 12 days. The hydrogels obtained showed potential for use in the biomedical area.
*Keywords*: antimicrobial, biocompatibility, chitosan hydrogel, *R. officinalis* extract, wound dressing.

## Resumen
El estudio de la modificación de hidrogeles por tecnología de plasma es relevante para los investigadores debido a sus posibles aplicaciones biomédicas. Esta investigación tiene como objetivo la modificación de hidrogeles de quitosano/*Rosmarinus officinalis* extract, que ayude a convertirlo en un hidrogel con potencial aplicación como apósito de heridas. Se fabricaron diferentes hidrogeles de quitosano/*R. officinalis*, modificados con plasma a 100, 150 y 200 W. Se evaluaron sus propiedades de biocompatibilidad y efecto antimicrobiano, además, fueron caracterizados mediante FTIR, TGA, DSC y SEM, y evaluados por su capacidad de degradación, hinchamiento y liberación de extracto. Los hidrogeles modificados con plasma a 200 W obtuvieron una biocompatibilidad superior, presentando una viabilidad celular >80% y un porcentaje de hemólisis <2%, para las concentraciones evaluadas de 1 y 2,5 mg/mL del material, a su vez, presentaron mayor efecto antimicrobiano contra *S. aureus* y *E. coli*, en comparación con los hidrogeles modificados a 100 y 150 W. Al mismo tiempo, se obtuvo un mayor porcentaje de liberación de extracto de *R. officinalis* en los hidrogeles con un tratamiento plasmático de 200 W, logrando una liberación sostenida hasta por 12 días. Los hidrogeles obtenidos presentaron potencial para ser utilizados en el área biomédica.
*Palabras clave*: antimicrobiana, biocompatible, hidrogel de quitosano, extracto de *R. officinalis*, apósito de heridas.

*Corresponding author. *E-mail*: rinarro@uadec.edu.mx;
https://doi.org/10.24275/rmiq/Poly24171
*ISSN*:1665-2738, *issn-e*: 2395-8472

# 1 Introduction

The largest organ in the human body is the skin, serving as a protective shield against external harm or danger (Yuan *et al*., 2022). Skin lesions have arisen as a health concern, as they have become a significant issue. A severe injury is difficult to treat and can be a source of life-threatening bacterial infections (Zhu *et al*., 2022). The primary method for treating damaged skin is the use of versatile wound dressings. They act as an antibacterial barrier essential for skin wound repair and tissue reconstruction (Yuan *et al*., 2022). A dressing with antimicrobial properties helps speed wound healing. Biomedical materials are periodically loaded with antibiotics to gain antimicrobial properties, but long-term use results in the emergence of some drug-resistant bacteria (Ge *et al*., 2022).

Natural extracts with antimicrobial properties are being used as an alternative to conventional antibiotics. *R. officinalis* has been used since ancient times to treat various conditions, as it is antioxidant, antimicrobial, antispasmodic, antirheumatic, diuretic, antidiabetic, antiepileptic, antidepressant, hepatoprotective, with anticancer activities and to improve memory dysfunction (Karadağ *et al*., 2019). The diverse components of *R. officinalis* are responsible for its biological activities: flavonoids, monoterpenes, diterpenes, sesquiterpenes, alcohols, esters, ketones, and hydrocinnamic derivatives (Ali *et al*., 2019). The main phenolic diterpenes are carnosol and carnosic acid (Sadeghi *et al*., 2022). Other less predominant components, such as epirosmanol, epiisorosmanol, carnosol quinone, methyl carnosate, rosmadial, and rosmanol could significantly influence some biological activities related to *R. officinalis* extracts (Sánchez-Camargo and Herrero 2017). Studies have indicated that the most potent antibacterial fractions of *R. officinalis* extract, obtained using organic solvents through ultrasonication, impregnation, or other methods, are mainly composed of non-volatile compounds (Zhong *et al*., 2020).

Various types of wound dressings have been designed, such as nanofibers, foam membranes, and hydrogels, among others (Deng *et al*., 2022). A hydrogel is characterized by being a soft material with a three-dimensional network structure. These materials have the ability to retain significant volumes of water and exhibit porosity and biocompatibility. Hydrogels for wound dressings support a highly humid environment, promote wound protection against microorganisms and bacterial infections, and have good oxygen-penetrating properties (Yuan *et al*., 2022).

Hydrogels can be made from natural polymers such as gelatin, cellulose, sodium alginate, chitosan, and hyaluronic acid, as they have excellent biocompatibility and biodegradability properties (Deng *et al*., 2022). Chitosan is a natural amino polysaccharide obtained through the deacetylation of chitin; its chemical name is poly-glucosamine (1-4)-2-amino-$\beta$-D-glucosamine (Guo *et al*., 2022; Zapata-Luna *et al*., 2023), and it has biocompatibility properties (Rodríguez-Guzmán *et al*., 2022), biodegradability, non-toxicity, mucoadhesive and antimicrobial properties (Tran *et al*., 2020, Rezaei *et al*., 2021). Chitosan can form a gel in situ, sensitivity to pH, straightforward adaptability, and compatibility for crosslinking with various polymers (Yan *et al*., 2022). It has good mechanical properties thanks to its linear, unbranched, and high molecular weight structure (Feng *et al*., 2021). Chitosan is not soluble in aqueous media, so it requires an acid medium with a pH below 6 to dissolve due to the protonation of the amino groups of the chitosan chains (Maiz-Fernández *et al*., 2020).

Although it is reported that a hydrogel derived from chitosan exhibits favorable biocompatibility properties, plasma technology can still improve these properties. This technology modifies surfaces with a shorter functionalization time, implementing green chemistry principles, and avoiding waste. Plasma is the fourth state of matter (Chytrosz-Wrobel *et al*., 2023), is a partially ionized gas that contains excited and unexcited free electrons, ions, radicals, molecules, and photons and carries a net neutral charge (Bao *et al*., 2020, Okyere *et al*., 2022). Low pressure is commonly employed in biomaterials research because the discharge is more stable than in atmospheric pressure plasmas, and plasma reactions can be more easily controlled. Various plasma treatment processes can occur depending on the interaction between the substrate surface and the low-pressure plasma, such as polymerization (deposition of thin films of polymers at nanoscale, in a homogeneous and controlled manner) (Akther *et al*., 2023; Navascués *et al*., 2023), sterilization, erosion (spraying of the upper layer of the material) (Kumar *et al*., 2021) or activation (gases anchor functional groups on surfaces and improve their surface adhesion in plasma activation). If a monomer is used, a polymeric layer can be formed, grafting polymers to the substrate or inducing surface hydrophilicity by introducing polar groups on the surface of the substrate (Sundriyal *et al*., 2021). This last strategy is used to a large extent to achieve antimicrobial activity since the functional groups or free radicals generated on the surface through plasma treatment act as binding sites to incorporate antibacterial agents, such as antibiotics, and enzymes that dissolve biofilms, among others (Akdoğan and Şirin 2021).

The objective of this research was to develop

chitosan hydrogels with different concentrations of *R. officinalis* extract and to modify them by means of plasma technology applying three potencies as a strategy to improve their biocompatibility properties, which could be helpful for future biomedical applications such as the use of wound dressings, where so far there are no reports in the literature of hydrogels morphologically modified with radiofrequency plasma.

## 2 Materials and methods

### 2.1 Materials

The reagent ethyl acetate ($CH_3COOC_2H_5$), ≥ 99.5% used to obtain bioactive compounds from *R. officinalis*, was acquired from Sigma Aldrich. *R. officinalis* was obtained from a shrub (in Ramos Arizpe, Coahuila, Mexico) eight years old, measuring 1 m and 10 cm. At the time of its collection, the shrub was not in bloom, with which the Materials Science and Technology Department has been working. The reagents for hydrogel synthesis were purchased from Sigma Aldrich and were used without additional treatment: high molecular weight chitosan (300 KDa, deacetylated chitin, Poly (D-glucosamine)), glacial acetic acid ($CH_3COOH$, 99.98%) and sodium hydroxide (NaOH 98%).

### 2.2 Extraction of bioactive compounds from R. officinalis

Fresh *R. officinalis* was washed with tap water and dried at room temperature in the open air for five days. The dried *R. officinalis* leaves were placed in test tubes containing 5,000 mg of *R. officinalis* leaves, and 50 mL of ethyl acetate was added. The test tubes were subjected to ultrasonic radiation in a BRANSSON 5500 ultrasonic bath at a frequency of 40 to 60 kW for 60 minutes. Once the time was over, the *R. officinalis* leaves were discarded, and the solvent was poured into Petri dishes, where it was dried at room temperature, leaving only the *R. officinalis* extract on the Petri dish.

### 2.3 High-Performance Liquid Chromatography (HPLC) of R. officinalis extract

The reversed-phase high-performance liquid chromatography analysis derives its name from the fact that ionic and highly polar analytes are the first to elute on the column, followed by the more hydrophobic analytes. This analytical process was conducted using a Varian HPLC system, which includes a sampler (Varian ProStar 410, USA), a ternary pump (Varian ProStar 230I, USA), and a PDA detector (Varian ProStar 330, USA). This equipment is equipped with a liquid chromatography ion trap mass spectrophotometer that features an electrospray ion source. Samples (5 $\mu$L) were injected into a Denali C18 hydrophobic column (150 mm x 2.1 mm, 3 $\mu$m Greece, USA). The oven temperature was held at 30 °C. Formic acid (0.2%, v/v, solvent A) and acetonitrile (solvent B) were employed as eluents. The following gradient was applied: initial, 3% B, 0-5 min, 9% B linear, 5-15 min, 16% B linear, 15-45 min, 50% B. Subsequently, the column was washed and reconditioned. The flow rate was maintained at 0.2 mL/min, and the elution was monitored at 245, 280, 320, and 550 nm. All eluent (0.2 mL/min) was directed into the mass spectrometer source without splitting. The experiments were conducted in negative $[M-H]^{-1}$ mode. Nitrogen served as the nebulizer gas and helium as the buffer gas. The Ion Source parameters were set at a spray voltage of 5.0 kV, and voltage and temperature of 90.0 V and 350 °C, respectively. Data collection and processing were performed using MS workstation software (V 6.9). The samples were initially analyzed in full scan mode within the m/z 50 - 2000 range.

### 2.4 Hydrogel synthesis

For hydrogel preparation, the methodology used by Lu *et al*., 2022 (Zhengbo *et al*., 2022) by modifying the stirring time, temperature, and NaOH concentration according to (Ahmed Mohamed *et al*., 2021). Hydrogels loaded with *R. officinalis* extract were prepared similarly, but adding *R. officinalis* extract to the chitosan solution with the following concentrations 0.005, 0.025, and 0.05 mg/mL.

### 2.5 Modification of hydrogels with plasma technology

Plasma treatment was performed in a plasma reactor with radiofrequency at 13.56 MHz, using air as a resource. Treatments were performed at 100, 150, and 200 W, at a pressure of 0.45 mbar for 30 min.

### 2.6 Structural characterization of the hydrogels

The infrared spectra were obtained using the attenuated total reflection technique (FTIR-ATR) with a Thermo Scientific Nicolet iS10 instrument, covering a range of 600 to 4000 $cm^{-1}$, 100 scans, and a resolution of 0.4 $cm^{-1}$.

The morphological characterization of the hydrogels was performed on an SEM field emission scanning electron microscope. The samples were coated with gold nanoparticles to facilitate electrical conductivity before analysis.

Table 1 shows the nomenclature used for the hydrogels obtained and modified with plasma.

| Name of chitosan hydrogel | Power used for plasma modification (W) | Concentration of *R. officinalis* extract (mg/mL) |
|---|---|---|
| HCS0.0 | — | — |
| HCS1.100 | 100 | 0.005 |
| HCS1.150 | 150 | 0.005 |
| HCS1.200 | 200 | 0.005 |
| HCS2.100 | 100 | 0.025 |
| HCS2.150 | 150 | 0.025 |
| HCS2.200 | 200 | 0.025 |
| HCS3.100 | 100 | 0.05 |
| HCS3.150 | 150 | 0.05 |
| HCS3.200 | 200 | 0.05 |

*—: Without plasma modification and without *R. officinalis* extract.

The thermal properties of the biocomposites were analyzed on a Shimadzu DSC-60 differential scanning calorimeter. Initially, heating was performed at 20 °C/min from 30 to 200 °C, and the temperature was maintained at 200 °C for 1 min to erase the sample's thermal history. Subsequently, the samples were cooled at 20 °C/min to 30 °C.

Thermogravimetric analyses were performed on a Perkin Elmer TGA 4000. The analyses were carried out in an inert atmosphere of $N_2$, with a heating rate of 20 °C/min, from 30 to 800 °C.

## 2.7 Degradation and swelling test

The degradation and swelling test of the hydrogels was conducted by immersing them at room temperature and using solutions with different pH for 30 days. The following solutions were used for the analysis: NaOH (pH=12), HCl (pH=2), and PBS (pH=7.4). This study evaluated the difference in the total mass of the hydrogel during the immersion time.

The following equation (Eq. 1) was used to determine the mass variation of the hydrogels.

$$\text{Mass variation } (\%) = \left(\frac{m_x - m_0}{m_0}\right) \times 100 \qquad (1)$$

Where $m_x$ is the mass of the hydrogel at a given time ($x$=day), and $m_0$ is the initial mass of the hydrogel.

## 2.8 R. officinalis extract release test

To analyze the release of *R. officinalis* extract in each hydrogel, this was immersed in 10 mL of the PBS solution, pH 7.4 at 25 °C. At different time intervals, 1 mL aliquots of the release medium were measured, and an identical volume of PBS was added. The concentration of *R. officinalis* extract released into the medium was quantified at 240 nm, according to the maximum peak in the 200 to 700 nm run. The percentage of loading and release was calculated based on the calibration curve, plotted using standard solutions of increasing concentrations of *R. officinalis* extract.

## 2.9 Cytotoxicity tests

### 2.9.1 In vitro hemolysis test

The hemolytic activity assay was employed to assess the blood compatibility of the hydrogel (Deng *et al*., 2022). Erythrocytes were extracted from fresh blood, and subjected to three washes with Alsever solution, and the erythrocytes were diluted in Alsever solution to a concentration of 10% (v/v). In a culture plate, 1500 $\mu$L of the erythrocyte suspension was blended with the hydrogel at concentrations of 1, 2.5, and 5 mg/mL. Alsever solution served as a negative control, while distilled water acted as a positive control. Following a 1-hour incubation at 37 °C with agitation at 100 rpm, the mixture underwent centrifugation at 2500 rpm for 4 minutes. Subsequently, 1000 $\mu$L of supernatants were transferred to a new transparent 24-well plate, and the absorbance of the solutions was measured at 415 nm using a Sinergy HTX model microplate reader. Each group underwent three repetitions, and the hemolysis rate was calculated using the following:

$$\%\ \text{Hemolysis} = \frac{(\text{A sample} - \text{A negative control}) \times 100}{\text{A positive control} - \text{A negative control}} \qquad (2)$$

Note: A = absorbance.

### 2.9.2 Cell viability test

Cytotoxicity testing of the hydrogels was conducted through the (3-(4,5-dimethylthiazol-2-yl)-2,5-diphenyltetrazolium bromide) (MTT) assay, employing mouse fibroblast 3T3 cells. These cells were cultured in 3 mL of medium at 37 °C under a 5% $CO_2$ atmosphere for 5 days. Subsequently, the cells were seeded into a 96-well plate with 200 $\mu$L of medium at a density of 8,500 cells per well and allowed to settle for 24 hours. The samples for evaluation were prepared under conditions of 5°C and a 5% $CO_2$ atmosphere. A solution containing complete culture medium was prepared in contact with the

different hydrogels obtained and allowed to react for 24 hours. Subsequently, the solution was removed and placed in contact with the cells. They have incubated again at 37 °C, with a 5% $CO_2$ atmosphere for 24 h. A negative control consisting of 200 $\mu$L of culture medium and a positive control of 20 $\mu$L of 100x newt solution were used. After removing the culture medium, 20 $\mu$L of MTT solution was added to the plates. The 96-well plates with the cell culture and samples were incubated for 4 hours at 37 °C under a 5% $CO_2$ atmosphere. Subsequently, the medium was carefully removed, and 100 $\mu$L of (DMSO) was added to crystallize the formazan and quantify the color. Absorbance readings were taken using a Thermo Scientific MultiScan FC UV-vis spectrophotometer at a wavelength of 570 nm. Before adding the MTT reagent, brightfield photographs were captured at 40X magnification under an inverted microscope to assess the cell morphology. The percentage of cell viability of the samples was calculated using Equation 3:

$$\%CV = \frac{AS}{ANC} \times 100 \tag{3}$$

Where: CV = cell viability, AS = Absorbance of the sample, ANC = Absorbance of the negative control.

### 2.10 *Qualitative antibacterial assay*

The antimicrobial properties of the hydrogels were investigated with a qualitative assay using the halo formation inhibition method. Two clinical pathogenic bacterial strains were chosen, one Gram-positive (*S. aureus*) and one Gram-negative (*E. coli*). The microbiology laboratory of the Universidad Autónoma de Coahuila provided these strains. Antibiogram-type *in vitro* antibiosis bioassays were performed using serial dilutions. For inoculation, the dilution ($1\times10^{-3}$) was used, 200 $\mu$l of nutrient agar boxes were placed, seeded uniformly, and then one chitosan hydrogel/*R. officinalis* per box was placed, previously sterilized by irradiation with ultraviolet light for 20 min. A chitosan hydrogel without *R. officinalis* extract was used for the absolute control. Each hydrogel had a diameter of 7 mm. The boxes were incubated for 24 h at a temperature of 37 ºC. Once the incubation time had elapsed, the inhibition halos formed could be observed. This procedure was performed in triplicate.

### 2.11 *Statistical analyses*

All statistical analyses were performed with a one-way analysis of variance (ANOVA) followed by Tukey's test. Experiments were carried out in triplicate independently and in turn, three replicates (n=9) were performed. The multiple comparison tests evaluated the significant difference between treatments, and a value of $p<0.05$ was considered statistically significant.

## 3 Results and discussions

### 3.1 *HPLC of R. officinalis extract*

The composition of *R. officinalis* extract underwent evaluation through HPLC. The mass spectrometric analysis of the chromatogram revealed a variety of components, encompassing flavones, methoxy flavones, flavonols, lignins, hydroxycinnamic acids, phenolic terpenes, and anthocyanins, among others. Among these compounds, certain constituents appeared in higher concentrations, including catechins at 5.58% with a retention time (RT) of 16.99 min, caffeic acid at 9.08% with a RT of 26 min, jaceosidine at 1.63% with a RT of 31.54 min, cyanidin-3,5-O-diglucoside at 6.46% with a RT of 39.33 min, cyrsimaritin at 1.37% with a RT of 49.64 min, and rosmanol at an impressive 13.86% with a RT of 57.9 min. Notably, rosmanol emerged as the most prevalent compound, signifying its significance as one of the primary constituents conferring antioxidant properties to the *R. officinalis* extract (Embuscado 2015). Table 2 offers an overview of the major extracted compounds. Given that this chromatography employed reverse-phase methodology, compounds with greater polarity materialized at shorter retention times, while less polar compounds surfaced at longer retention times. A study by Tzima *et al.* in 2021 assessed *R. officinalis* extract constituents extracted via ultrasound using 55.91% ethanol. This research identified various compounds, including flavones (luteolin), methoxyflavones (cyrsimaritin), flavanones, flavonols, phenolic terpenes (rosmanol), phenolic acids, hydroxybenzoic acid, hydroxycinnamic acid (caffeic acid), and lignans. Interestingly, these compounds, noted by earlier researchers, aligned with some of the compounds extracted from *R. officinalis* in this study. However, distinctions arose, such as the presence of valinic acid, coumaric acid, rosmarinic acid, and rosmadial in Tzima *et al.* report. This divergence likely stemmed from the use of a polar extraction solvent in that study, leading to the extraction of more polar compounds. In the current investigation, ethyl acetate served as the extraction solvent, yielding not only similar compounds but also additional constituents like catechins, methoxyflavones (jaceosidin), flavonols (quercetin), and lignins (lariciresinol), among others (Tzima *et al.*, 2021).

Table 2. Quantification of *R. officinalis* extracts by HPLC.

| Retention time (RT) (min) | Mass (mg/g) | Percentage present in the extract (%) | Compound | Family |
|---|---|---|---|---|
| 16.99 | 289.3 | 5.58 | Catechins | Catechins |
| 25.83 | 178.9 | 9.08 | Caffeic acid | Hydroxycinnamic acids |
| 25.83 | 135 | 1.96 | p-Anisaldehyde | Methoxybenzaldehydes |
| 31.54 | 329 | 1.63 | Jaceosidine | Methoxiflavones |
| 31.54 | 964.1 | 0.97 | Patuletin-3-O-(2-feruloylglucosyl)(1->6)-(apiosyl(1->2))-glucoside | Methoxyflavonols |
| 36.45 | 300.9 | 0.76 | Quercetin | Flavonols |
| 36.45 | 477.1 | 0.92 | Quercetin-3-O-glucuronide | Flavonols |
| 36.45 | 565.1 | 0.54 | Pelargonidin-3-O-sambubioside | Anthocyanins |
| 39.33 | 301 | 1.08 | 6-Hydroxyluteolin | Flavones |
| 39.33 | 609.2 | 1.27 | Quercetin-3-O-rutinoside | Flavonols |
| 39.33 | 610.1 | 6.46 | Cyanidin-3,5-O-diglucoside | Anthocyanins |
| 42.43 | 359 | 1.44 | Lariciresinol | Lignins |
| 43.87 | 653.1 | 0.87 | Maldivin-3,5-O-diglucoside | Anthocyanins |
| 43.87 | 654 | 1.39 | Maldivin-3-O-(6-caffeoyl-glucoside) | Anthocyanins |
| 46.74 | 285 | 1.72 | Luteolin | Flavones |
| 48.95 | 315 | 1.63 | Protocatechuic acid 4-O-glucoside | Hydroxybenzoic acids |
| 48.95 | 347 | 1.84 | 5-Heptadecylresorcinol | Alkylphenols |
| 49.64 | 161 | 0.78 | 4-Hydroxycoumarin | Hydroxycoumarins |
| 49.64 | 313.1 | 1.37 | Cyrsimaritin | Methoxyflavones |
| 52.63 | 329 | 0.89 | 3,7-dimethylquercetin | Methoxyflavonols |
| 57.9 | 345.1 | 13.86 | Rosmanol | Phenolic terpenes |

## *3.2 Characterization of chitosan hydrogels/R. officinalis modification by plasma technology*

### *3.2.1 FTIR-ATR spectrum*

Analysis of the FTIR-ATR spectrum, as illustrated in Figure 1, revealed several bands attributable to different bonds and functional groups present in the control chitosan hydrogel, the *R. officinalis* extract, and the different chitosan/*R. officinalis* hydrogels modified by plasma technology. The characteristic band of the O-H bond stretching is present at 3350 $cm^{-1}$, and at 3200 $cm^{-1}$, a small N-H signal is also observed, which is not so evident as it overlaps with the O-H signal. The 1650 $cm^{-1}$ bands correspond to C=O and 1400 $cm^{-1}$ characteristic of C-N. Finally, the 1050 and 897 $cm^{-1}$ bands correspond to symmetric and asymmetric C-O and C-H vibrations. As for the signals of the *R. officinalis* extract (Figure 1 a), two peaks between 2900 and 2967 $cm^{-1}$, corresponding to $CH_2$, and a characteristic band at 1650 $cm^{-1}$, corresponding to C=O stretching, are appreciated. Notably, the spectra revealed common signals between the *R. officinalis* extract and chitosan, likely due to the presence of shared compounds in both entities. Subtle variations in the spectra were discernible due to the

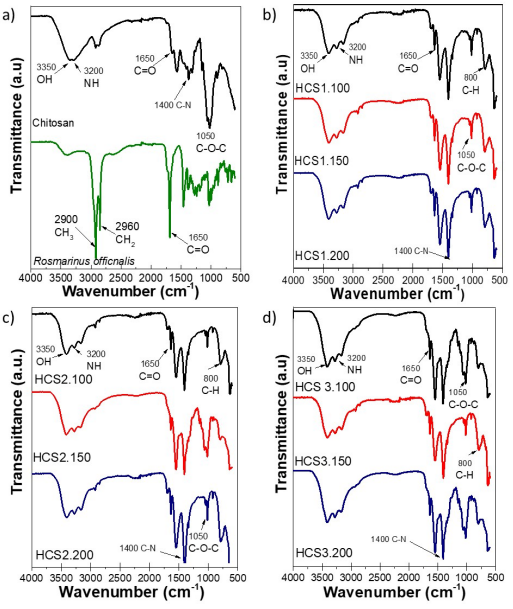


Figure 1. FTIR-ATR spectra: a) FTIR for pure chitosan and *R. officinalis* extract, b) chitosan hydrogels with 0.005 mg/mL *R. officinalis* extract and modified with plasma, c) chitosan hydrogels with 0.025 mg/mL *R. officinalis* extract and modified with plasma d) chitosan hydrogels with 0.05 mg/mL *R. officinalis* extract and modified with plasma.

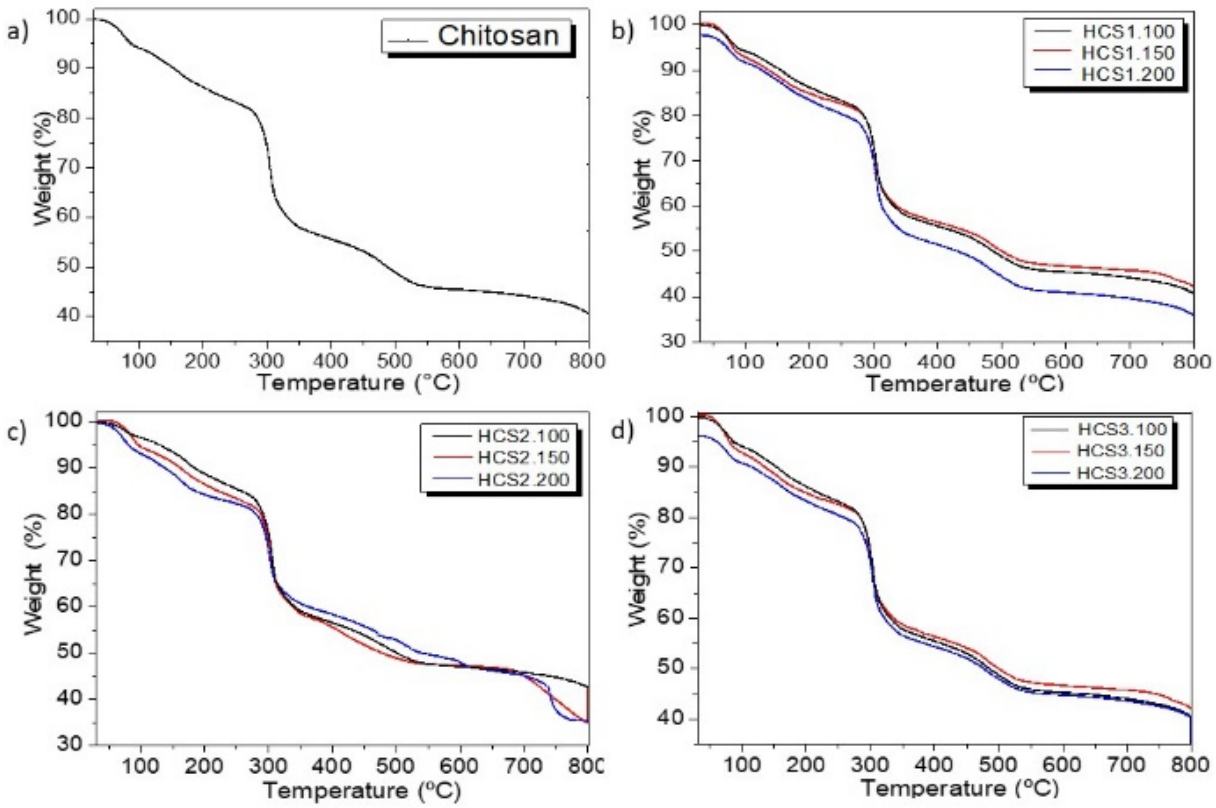


Figure 2. TGA curve of chitosan hydrogels. a) chitosan hydrogel, b) chitosan hydrogels with 0.005 mg/mL *R. officinalis* extract, c) chitosan hydrogels with 0.025 mg/mL *R. officinalis* extract, d) chitosan hydrogels with 0.05 mg/mL *R. officinalis* extract.

inclusion of the extract in the hydrogel. Remarkably, the plasma treatment effect did not yield significant alterations in the spectra.

### *3.2.2 TGA of hydrogels*

Figure 2 illustrates the thermogravimetric analyses obtained from the chitosan hydrogels: HCS0.0 (Control) and chitosan/*R. officinalis* hydrogels. In all samples, an initial weight loss of approximately 5-7% is observed starting at 100°C. This weight reduction is attributed to the physical absorption of water, given that chitosan is a hygroscopic material (Shrivastav *et al*., 2020). Beyond 200°C, a second weight loss of approximately 60% is evident, attributed to the pyrolysis of the biopolymer. During this phase, glycoside bonds break, followed by an oxidation process occurring between 450 and 620°C, culminating in the degradation of chitosan at 620°C (Bonilla-Cruz *et al*., 2017).

In this TGA analysis (Figure 3 b, c, and d), we observe a decrease in thermal stability in the chitosan hydrogels as the plasma treatment power increases. This decline in thermal stability could be linked to the rise in hydrogel porosity resulting from the increased plasma treatment power. This effect on porosity is also apparent in the SEM characterization (Section 3.3.4), where an increase in pores within the hydrogel is evident with higher power levels during plasma treatment (Corazzari *et al*., 2015). As for the concentration of *R. officinalis* extract present in the hydrogel, it can be inferred that the second weight loss, occurring around 300°C, corresponds to the pyrolysis of chitosan and the chemical bonds associated with the *R. officinalis* extract.

### *3.2.3 DSC of hydrogels*

Figure 3 illustrates the distinctive thermograms of various chitosan hydrogel samples, including the control (HCS0.0) and those derived from different concentrations of *R. officinalis* extract (0.005, 0.025, and 0.05 mg/mL), subjected to varying plasma treatment powers (100, 150, and 200 W).

In the thermographs, we observe endothermic peaks occurring within the temperature range of 40 to 65 °C, attributed to moisture evaporation (Dong *et al*., 2004). These peaks represent the energy needed for water evaporation within the chitosan hydrogel. The second distinct event, occurring at around 100 °C, is associated with the glass transition temperature (Tg) of chitosan (as depicted in Figures 3a and 3b). Although the Tg signal for chitosan is not always evident, numerous studies have pinpointed its presence within the range of 100 to 150 °C (Corazzari *et al*., 2015).

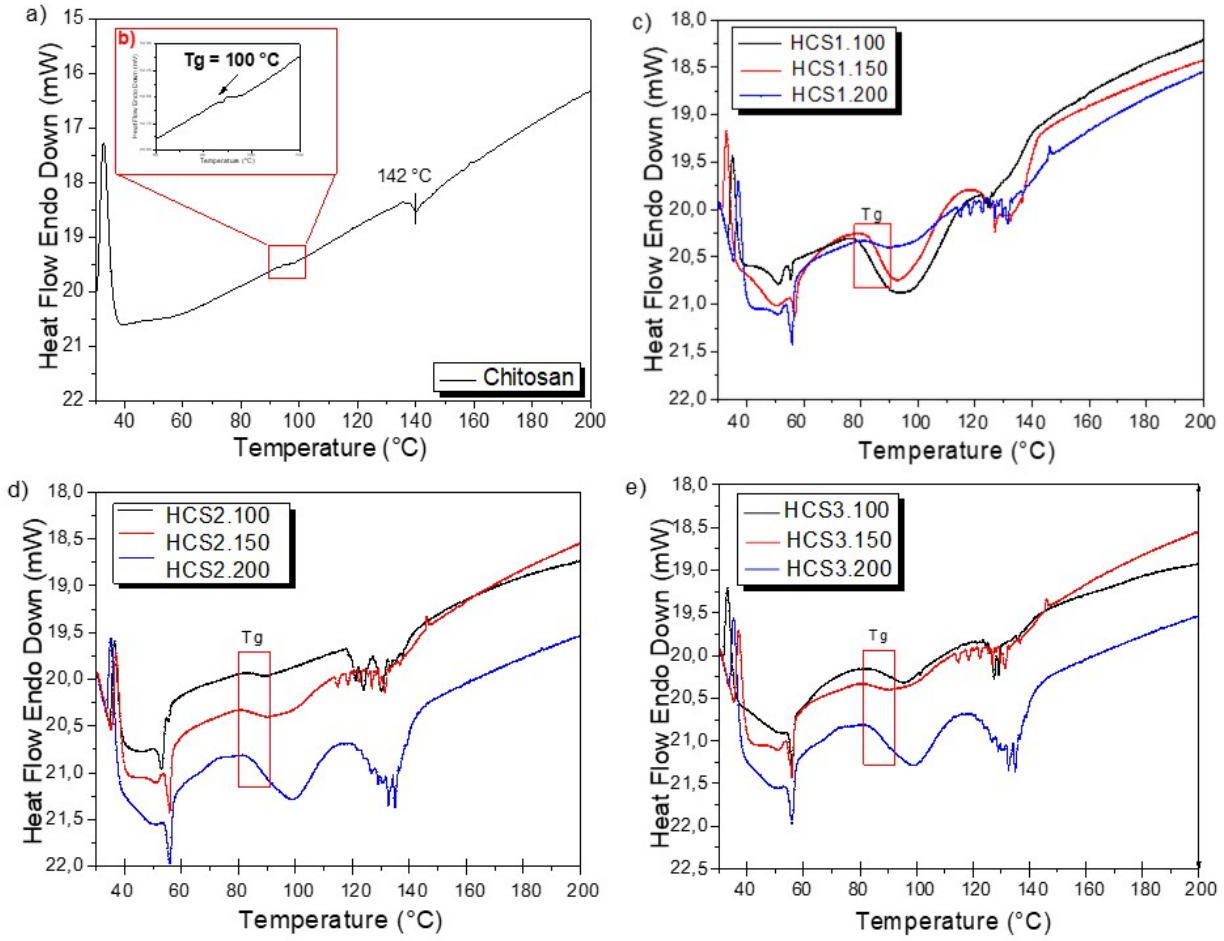


Figure 3. DSC curve of chitosan hydrogels. a) chitosan hydrogel, b) glass transition temperature of chitosan, c) chitosan hydrogels with 0.005 mg/mL *R. officinalis* extract, d) chitosan hydrogels with 0.025 mg/mL *R. officinalis* extract, e) chitosan hydrogels with 0.05 mg/mL *R. officinalis* extract.

Additionally, the melting temperature (Tm) is evident in the thermographs by an endothermic peak, typically around 142 °C (as seen in Figures 3a and 3b), resulting from the dissociation of hydrogen bonds between chitosan chains, created at the amino group and a hydroxyl functional group (Li Shan *et al*., 2021).

Figures 3 c, d, and e show the different thermograms of chitosan hydrogels varying the concentration of *R. officinalis* extract. The thermograms of HCS1, HCS2, and HCS3 present some differences concerning the thermogram of pure chitosan (Figure 3 a and b). For the hydrogel with 0.005 mg/mL of *R. officinalis* extract (Figure 3 c), a clear Tg signal is observed as the plasma power increases from 100 to 200 W. However, this signal moves to a lower temperature range, around 89 °C, compared to the pure chitosan that presents a Tg of 100 °C. This trend is similar for HCS2 (Figure 3 d) and HCS3 (Figure 3 e). This could be attributed to the increase in porosity after plasma treatment, which could result in a decrease in molecular weight, which is a factor for the reduction of Tg (Akihiro *et al*., 1992).

Regarding the melting temperature (Tm) of HCS1, HCS2, and HCS3, several peaks forming a broad melting band are observed around 120 to 140 °C, indicating a decrease in this temperature, compared to pure chitosan hydrogel (Tm =142 °C). These results generally indicate that chitosan loses thermal stability due to the *R. officinalis* extract content and the plasma treatment applied to the different hydrogels. As a result, a decrease in Tg and Tm is obtained, mainly attributed to the increase in porosity after plasma treatment.

### *3.2.4 SEM of hydrogels*

Figure 4 illustrates SEM images, where panels a) and e) depict chitosan hydrogels without plasma modification; panels b) and f) show chitosan hydrogels subjected to plasma modification at 100 W; panels c) and g) represent chitosan hydrogels modified with plasma at 150 W, and panels d) and h) showcase hydrogels treated with plasma at 200 W. The analysis reveals a distinct morphology.

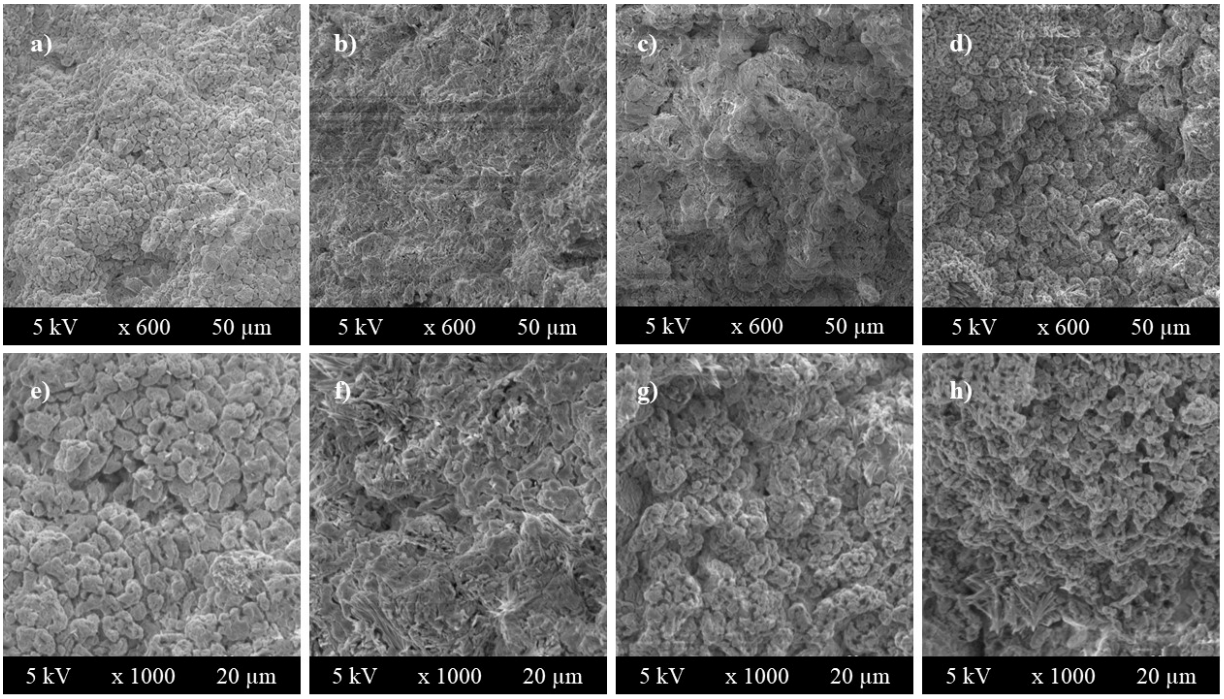


Figure 4. Scanning electron microscopy, for a) and e) HCS0.0; b) and f) HCS3.100; c) and g) HCS3.150; d) and h) HCS3.200.

Notably, the untreated hydrogel (panels a and e) exhibits a more compact structure compared to the modified counterparts. As the radiofrequency plasma power increases, observable pores emerge within the hydrogel structure. This phenomenon is likely a result of elastic impacts from charged species present in the plasma colliding with the material's surface and causing material detachment, a process known as the sputtering effect (Fridman 2023). It is worth noting that $OH^-$ and $H_3O^+$ species, being the most abundant charged species in air plasma, could be responsible for modulating this effect through their pH influence (Aflori *et al*., 2015; Levin *et al*., 2023; Pérez-Huertas *et al*., 2024; Wiącek *et al*., 2018).

According to Fridman, this alteration in plasma pH can be attributed to material detachment through particle collision, resulting in the distinctive surface morphology observed in the hydrogel (Fridman 2008). Previous research has indicated that plasma treatment utilizing residual air as a resource can lead to surface erosion, which is readily apparent through microscopy (Fridman 2008).

### *3.3 Degradation and swelling test*

In this section, we present the results of the mass gain or loss observed in chitosan hydrogels when exposed to solutions of varying pH levels. The water absorption properties of these hydrogels are influenced by their interconnected network, pore distribution, and other factors, including pH, which play a significant role in their swelling behavior (Niladri Sekhar *et al*., 2022). Chitosan and its derivatives exhibit inherent pH sensitivity, and their solubility is contingent upon pH conditions. Specifically, in neutral and alkaline solutions, chitosan exhibits poor solubility and diminished mechanical performance due to the deprotonation of its amino groups. Conversely, at lower pH levels, the polymer chains can expand easily, and the amino groups become protonated (Singha and Basu 2022). These characteristics enable us to predict the swelling behavior of hydrogels, irrespective of the specific drugs or active substances they might contain (Li Shan *et al*., 2021).

Chitosan hydrogels immersed in an HCl solution with a pH of 2.0 underwent rapid degradation, with a 100% weight loss observed within 24 hours (Figure 5a). This phenomenon occurs because chitosan, which is soluble in media with a pH below 6, dissolves due to the protonation of the amino groups in the chitosan chains (Maiz-Fernández *et al*., 2020). Figure 5b depicts the results of the swelling percentage of hydrogels immersed in a pH 7.4 solution. The highest value recorded was 324%, achieved on the fifth day by hydrogel HCS1.100. On the second day, all hydrogels at least doubled their initial mass. The swelling percentage increased progressively from day 1 until reaching its peak between days 5 and 9. In the case of hydrogels exposed to pH 12 (Figure 5c), all hydrogels exhibited a swelling percentage exceeding 900% on the third day. However, a decline in mass commenced the following day. After 30 days, the hydrogels still maintained a swelling percentage exceeding 400%. Although this value is substantial,

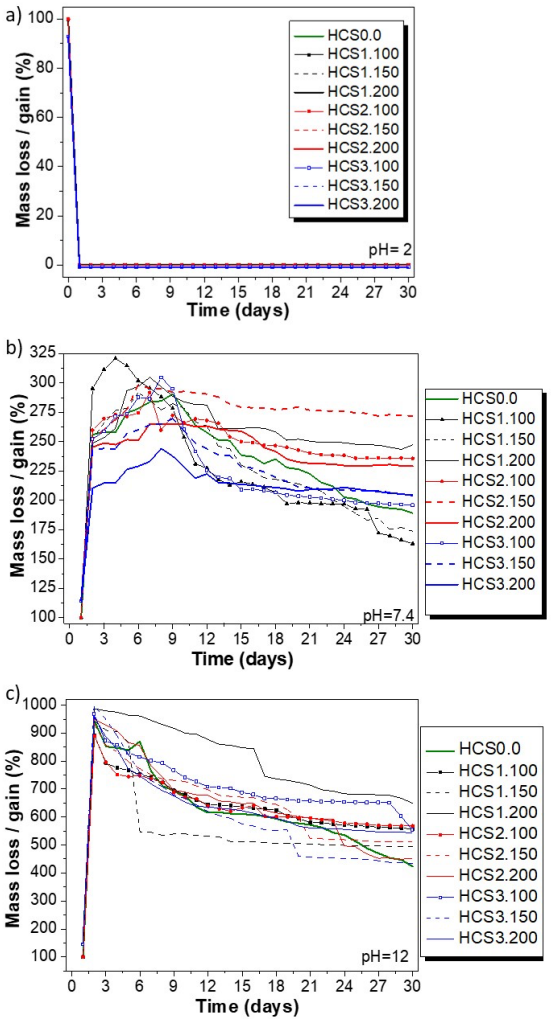


Figure 5. Percentage degradation and swelling of chitosan/*R. officinalis* hydrogels exposed to different pH.

it represents a decrease of more than 50% from the maximum value achieved. The swelling percentage of all hydrogels at pH 7.4 was lower compared to pH 12. The conclusion drawn was that the swelling percentage rises with increasing pH levels. This can be attributed to the formation of carboxylic anions within the polymer network, resulting in network expansion driven by strong electrostatic forces (Li Shan *et al*., 2021).

The graphs generated from the swelling and degradation tests offer comprehensive insights into the behavior of chitosan hydrogels exposed to different pH conditions, regardless of the active substances incorporated into the hydrogels. Chronic wounds typically exhibit an alkaline pH range between 7 and 9 (Zhu *et al*., 2020). Consequently, the results indicate that when exposed to this pH range, the hydrogel remains stable without degradation. This underscores the material's potential as a wound dressing, as it maintains the structural integrity of the hydrogel matrix while possessing the ability to absorb exudate

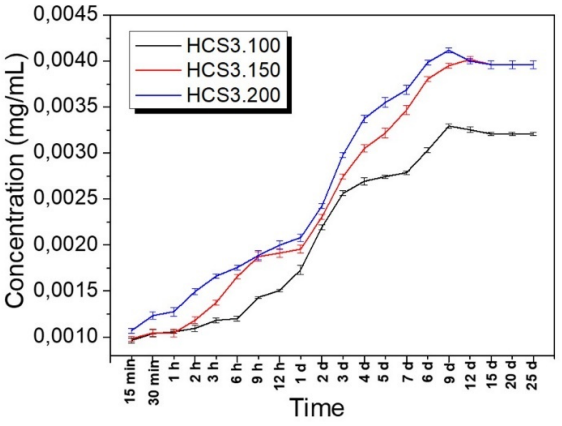


Figure 6. The concentration of *R. officinalis* extracts was released over 25 days.

or blood from the wound. It is important to note that these results represent a novel contribution, as they have not been previously reported in any research studies.

### *3.4 Release of R. officinalis extract*

The *in vitro* release behavior of *R. officinalis* extract in chitosan hydrogel was thoroughly investigated. The hydrogels under examination featured the highest concentration of *R. officinalis* extract (0.05 mg/mL) and had undergone modification through plasma technology (HCS3.100, HCS3.150, and HCS3.200). The results are illustrated in Figure 6.

The release of *R. officinalis* extract occurred in PBS at pH 7.4, and the release rate was graphed over time. The extract exhibited a gradual and sustained release pattern, commencing within the first 15 minutes and persisting until day 12 for all three hydrogel variants. Subsequently, there was a decline in the release rate, ultimately reaching a plateau at 16 days. It is worth noting that while the extract diffused from the hydrogel into the dissolution medium, a portion of the extract remained trapped within the hydrogel matrix.

This release behavior bears a resemblance to a similar study conducted by Li-Shan *et al*. in 2021, which involved the use of a chitosan hydrogel for evaluating the release of diclofenac sodium. In that study, the drug was gradually released, peaking at 16 hours, followed by a decrease in the release rate, ultimately reaching a plateau at 32 hours (Li-Shan *et al*., 2021). In contrast, in our present investigation, we achieved a release duration of 12 days, as opposed to Li-Shan *et al*., who only attained 16 hours of sustained release.

The hydrogels HCS3.100, HCS3.150, and HCS3.200 exhibited similar release behavior. The distinction among them lay in the maximum amount of extract they released. Specifically, HCS3.100 released 0.0033 mg/mL of extract, HCS3.150 reached

a maximum of 0.004 mg/mL, and HCS3.200 released 0.0042 mg/mL. This phenomenon can be attributed to the plasma modification process; a higher plasma modification potency resulted in a more pronounced release of *R. officinalis* extract. Presumably, the hydrogel modified with higher potency exhibited greater porosity, facilitating the passage and release of the *R. officinalis* extract. This effect was observed in the scanning electron microscopy images of the hydrogels.

## *3.5 In vitro hemolysis test*

Hemocompatibility refers to the interaction of a material with blood. When developing biomaterials for the human body, it is crucial to select biocompatible materials that interact harmoniously with blood cells. Chitosan is known to exhibit favorable hemocompatible properties (Madni *et al*., 2021).

To assess how biomaterials, behave when in contact with blood cells, a hemolysis test was conducted. This experiment sought to examine the influence of the *R. officinalis* extract within the hydrogels and the influence of plasma treatment at different potencies. Various concentrations of the biomaterial (1, 2.5, and 5 mg/mL) were examined for different hydrogel treatments.

Figures 7a and 7b illustrate the results for hydrogels with concentrations of 0.005 and 0.025 mg/mL of *R. officinalis* extract, respectively. It is evident that the biomaterials obtained were non-hemolytic for the assessed concentrations of 1 and 2.5 mg/mL. As per ASTM F 756-17, hemolysis percentages below 2 are considered non-hemolytic. However, for the concentration of 5 mg/mL, they exhibited hemolysis values ranging from 2 to 4%, indicating a slightly hemolytic response. Figure 8c displays the outcomes for hydrogels loaded with the highest concentration of *R. officinalis* extract (0.05 mg/mL) (HCS3.100, HCS3.150, HCS3.200). For the evaluated concentration of 5 mg/mL, these hydrogels primarily exhibited hemolysis. Conversely, at concentrations of 1 and 2.5 mg/mL, they displayed slight hemolysis or were non-hemolytic, with hemolysis percentages below 3%.

This figure also illustrates that the greater the plasma modification power applied to the hydrogel, the lower the percentage of hemolysis observed when in contact with red blood cells. Plasma treatment enhances the biocompatibility of biomaterials while leaving their mass and volume properties unaltered. These treatments facilitate polymer functionalization by introducing various surface elements such as amines, carbonyls, hydroxyls, and carboxyl groups. These elements improve the interaction between polymeric molecules and biological systems (Colín-Orozco; Reyna-Martínez *et al*., 2018).

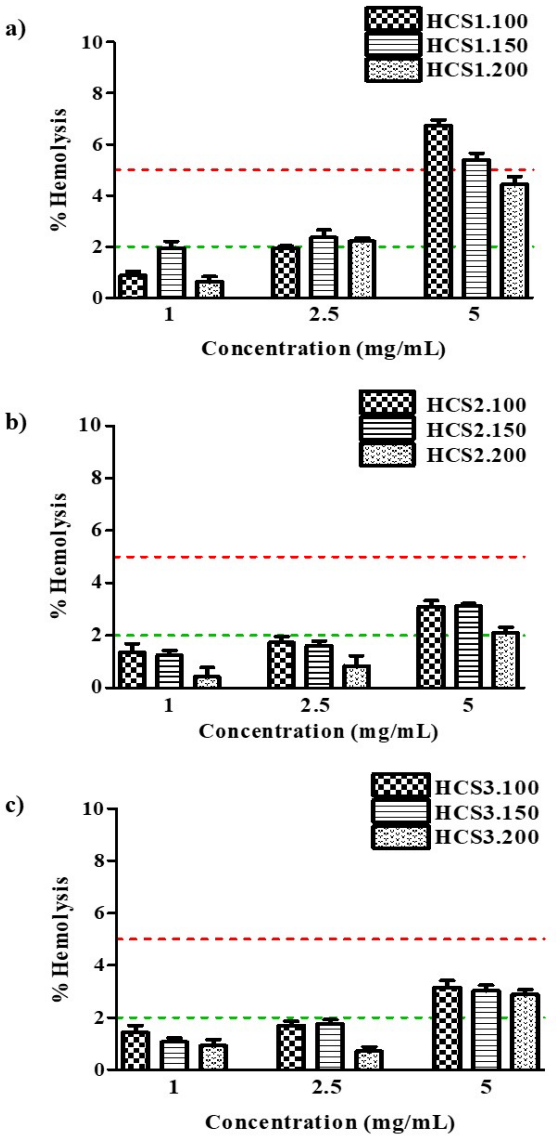


Figure 7. Hemolysis test a) chitosan/*R. officinalis* hydrogels (0.005 mg/mL); b) chitosan/*R. officinalis* hydrogels (0.025 mg/mL); c) chitosan/*R. officinalis* hydrogels (0.05 mg/mL).

Notably, the functional groups generated by air plasma predominantly include C-OH, C=O, HO-C=O, and $N_2$ (Men *et al*., 2022).

## *3.6 Cell viability assay (MTT)*

The viability of cells in chitosan hydrogels was evaluated through the MTT assay, a colorimetric technique that relies on the capacity of cellular mitochondrial dehydrogenases to transform yellow tetrazolium salt into purple formazan crystals (Constante *et al*., 2022). Figure 8 illustrates the cell cytotoxicity effect of chitosan hydrogel samples containing *R. officinalis* extract, with comparisons to a negative control of untreated cells (which exhibited 100% cell viability) and a positive control (Triton, a detergent) with less than 15% cell viability.

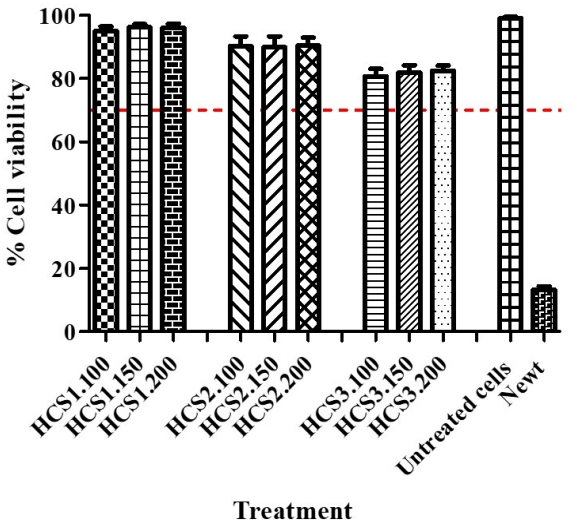


Figure 8. Percentage of cell viability with the different hydrogels obtained and the controls: untreated cells and triton.

Remarkably, all hydrogels displayed *in vitro* cell viability exceeding 80%.

According to ISO Standard 10993-5, a material with cell viability exceeding 70% is considered suitable for biomedical applications (10993-5:2009 ISO Standard, 2009). In a study by Mena-Huertas *et al*. in 2016, the cytotoxicity of *R. officinalis* was evaluated in human lymphocytes. They found that in its pure form, *R. officinalis* did not meet the safety criteria for biomedical use, as cell viability values fell below ISO 10993-5 standards. However, when different dilutions of *R. officinalis* (10-1, 10-2, 10-3) were tested, they complied with the percentage stipulated by the standard for safe biomedical applications (Mena-Huertas *et al*., 2016). The concentrations of *R. officinalis* used in the hydrogels did meet the parameters of the standard without the need for dilution; however, the results showed a decrease in the percentage of viability as the concentration of *R. officinalis* in the hydrogel increased.

The hydrogels containing 0.005 mg/mL of *R. officinalis* extract (HCS1.100, HCS1.150, HCS1.200) demonstrated cell viability percentages ranging between 95% and 96%. Hydrogels with 0.025 mg/mL of extract (HCS2.100, HCS2.150, HCS2.200) exhibited approximately 90% cell viability, while hydrogels with a higher concentration of *R. officinalis* extract (0.05 mg/mL) (HCS3.100, HCS3.150, HCS3.200) displayed slightly lower viability percentages, ranging between 80% and 82%.

There was no significant difference ($p<0.05$) observed between hydrogels loaded with the same concentration of *R. officinalis* extract but treated with varying plasma potencies. It was notable, however, that cell viability percentages decreased as the extract concentration increased. This suggests that, in eukaryotic cells, the application of aromatic plants may act as prooxidants rather than demonstrating their antioxidant properties. The cytotoxic effects on cells may vary depending on the type and concentration of the plant extract (Mena-Huertas *et al*., 2016).

The biocompatibility of the hydrogels is compromised by the concentration of *R. officinalis* extract present in the hydrogel since the concentration of chitosan was constant, and it is widely reported that chitosan is biocompatible (Huang *et al*., 2023; Sánchez-Armengol *et al*., 2024).

Figure 9 represents the photographs taken by optical microscopy at 40X of the hydrogels exposed to contact with the 3T3 cell line, where it is observed, the photograph of the untreated cells (negative control) compared to the photographs of the hydrogels at different concentrations of *R. officinalis* extract shows the same morphology since the cells are alive and comply with the percentages of cell viability established by ISO 10993-5. In contrast, destroyed cells are observed in the positive control (newt), a detergent in which cell death is provoked.

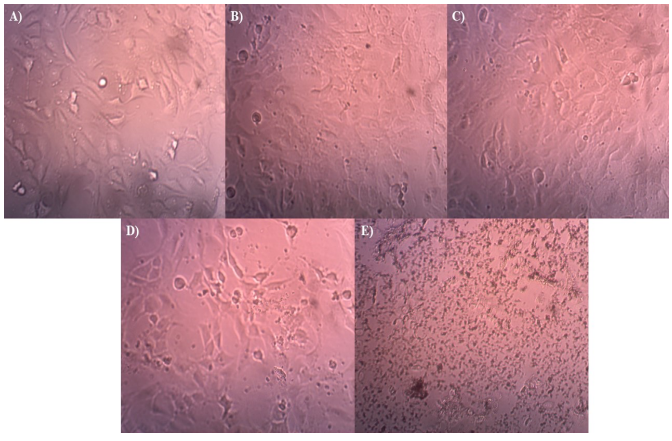


Figure 9. Photographs were taken by optical microscopy at 40X. A) hydrogel with 0.005 mg/mL *R. officinalis* extract, B) hydrogel with 0.025 mg/mL *R. officinalis* extract, C) hydrogel with 0.05 mg/mL *R. officinalis* extract, D) untreated cells E) newt.

### *3.7 Qualitative antimicrobial assay of chitosan hydrogels loaded with R. officinalis extract and modified by plasma technology*

In this qualitative assay, it was observed that the various chitosan/*R. officinalis* hydrogels exhibit antimicrobial activity against the *S. aureus* strain (Figure 10). All the evaluated treatments demonstrated inhibition zones when compared to the absolute control (HCS0.0), which displayed no antimicrobial activity against the *S. aureus* strain (Table 3). A similar effect was noted in the research conducted by Hernández *et al*., in 2011, where chitosan films without the addition of natural extracts (control) were tested against the *S. aureus* strain and did not produce an inhibition zone against the strain under examination. The authors mentioned that irrespective of chitosan's inherent antimicrobial properties, this activity occurs only upon direct contact with the active sites of chitosan, and no migration of active agents takes place through the agar medium (Hernández-Ochoa *et al*., 2011). Upon direct contact, chitosan binds to negatively charged components, disrupting the bacterial membrane and causing cell lysis and death (Liu *et al*., 2023).

In our study, it was observed that as the concentration of *R. officinalis* extract within the chitosan hydrogels increased, the size of the inhibition zone on the agar plates also increased. Furthermore, the results indicated that when the various chitosan/*R. officinalis* hydrogels were modified with plasma at a power of 200 W; inhibition zones expanded as well. This can be attributed to the presence of pores within the hydrogels that facilitated the release of the *R. officinalis* extract, imparting antimicrobial properties to each hydrogel. The *R. officinalis* extract contains phenolic compounds such as rosmanol and caffeic acid, along with tricyclic diterpenes, which contribute to its antimicrobial properties (Amaral *et al*., 2019). Chitosan's antimicrobial effect may be attributed to the interaction of $NH_3^+$ groups, which induce cell lysis in negatively charged membranes. This mechanism is particularly effective against gram-positive bacteria due to their negatively charged cell walls, primarily composed of teichoic acids (Campo Vera *et al*., 2017).

Table 3. Inhibition halos of chitosan hydrogels loaded with different concentrations of *R. officinalis* extract against *S. aureus* and *E. coli* strain.

| Hydrogel | Inhibition halo against *S. aureus* (mm) | Inhibition halo against *E. coli* (mm) |
|---|---|---|
| HCS0.0 | 0 | 0 |
| HCS1.100 | 16 | 13 |
| HCS1.150 | 18 | 14 |
| HCS1.200 | 24 | 16 |
| HCS2.100 | 20 | 14 |
| HCS2.150 | 21 | 16 |
| HCS2.200 | 22 | 17 |
| HCS3.100 | 22 | 14 |
| HCS3.150 | 23 | 17 |
| HCS3.200 | 25 | 19 |

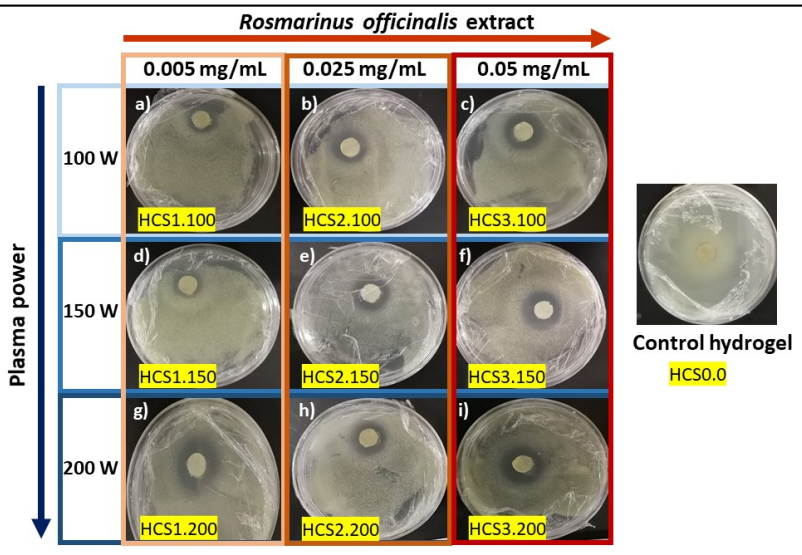


Figure 10. Inhibition halos of chitosan hydrogels loaded with different concentrations of *R. officinalis* extract against *S. aureus* strain.

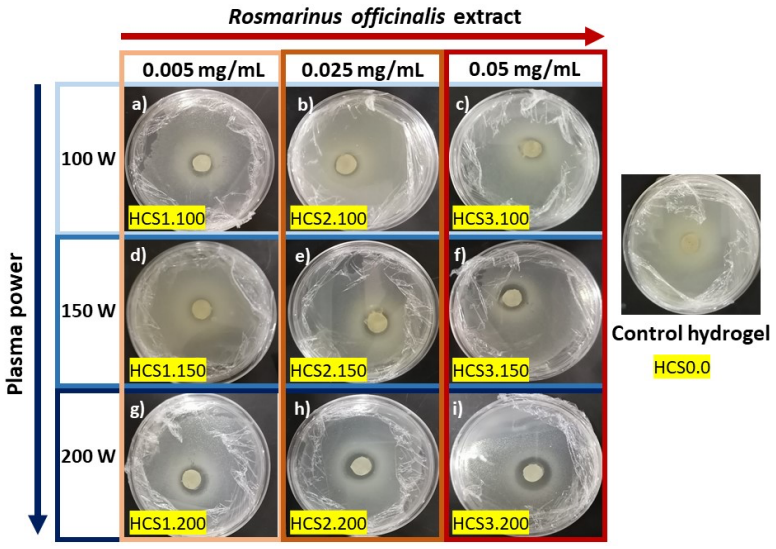


Figure 11. Inhibition halos of chitosan hydrogels loaded with different concentrations of *R. officinalis* extract against *E. coli* strain.

The plates inoculated with the *Escherichia coli* strain also exhibited inhibition zones (Table 4); however, the observed inhibition was not as pronounced when compared to the inhibition observed against *S. aureus*. The absolute control hydrogel showed no inhibition against the *E. coli* strain, in contrast to the chitosan/*R. officinalis* hydrogels, which displayed evident inhibition (Figure 11).

The results demonstrated a consistent trend for both the *E. coli* and *S. aureus* strains: the higher the concentration of *R. officinalis* extract and the more extensive the modification of the hydrogel with plasma technology, the larger the inhibition zone. Nevertheless, it is noteworthy that this inhibition effect was relatively reduced in comparison to gram-positive bacteria. Gram-positive bacteria tend to be more sensitive to the antimicrobial compounds found in chitosan and *R. officinalis* extract compared to gram-negative bacteria. This difference in sensitivity may be attributed to structural disparities between the two bacterial types, with the cell wall of gram-negative bacteria featuring an outer membrane rich in lipids, which provides protection to the integrity of their cell walls (Campo Vera *et al*., 2017).

## *Acknowledgment*

The authors thank the Mexican Council of Science and Technology (CONACYT) for the scholarship granted to Claudia Gabriela Cuéllar Gaona, CVU number 618041, for her doctoral studies.

## References

Aflori, M., Miron, C., Dobromir, M., and Drobota, M. (2015). Bactericidal effect on Foley catheters obtained by plasma and silver nitrate treatments. *High Performance Polymers 27*, 655-660. https://doi.org/10.1177/0954008315584171

Ahmed Mohamed, O., Wagih Abdel-Alim, S., Abdel-Ghaffar, M., and Heba Shawky, Hassan. Formulation of pH-sensitive aminated chitosan-gelatin crosslinked hydrogel for oral drug delivery. *Journal of Saudi Chemical Society 25*, 101384. https://doi.org/10.1016/j.jscs.2021.101384.

Akdoğan, E., and Şirin, H.T. (2021). Plasma surface modification strategies for the preparation of antibacterial biomaterials: A review of the recent literature. *Materials Science and Engineering: C 131*, 112474. https://doi.org/10.1016/j.msec.2021.112474

Akihiro, I., and Henning Winter, H. (1992). Molecular weight dependence of viscoelasticity of polycaprolactone critical gels. *Macromolecules 25*, 2422-2428. https://doi.org/10.1021/ma00035a020

Akther, H., Sheikh, M.S., Hussein, A.M., Hind, A., and Mahbubur, R.M. (2023). Insights into the structural and optical features of plasma polymerized N, N, 3, 5 tetramethylaniline-2,6-diethylaniline thin films. *Optical Materials 144*, 114278. https://doi.org/10.1016/j.optmat.2023.114278

Ali, A., Chua, B.L., and Chow, Y.H. (2019). An insight into the extraction and fractionation technologies of the essential oils and bioactive compounds in *Rosmarinus officinalis* L. Past, present and future. *TrAC Trends in Analytical Chemistry 118*, 338-351. https://doi.org/10.1016/j.trac.2019.05.040

Amaral, G., Mizdal, C., Stefanello, S., Mendez, A.S., Puntel, R.L., de Campos, M.M., and Soares, F.A., Fachinetto, R. (2019). Antibacterial and antioxidant effects of *Rosmarinus officinalis* L. extract and its fractions. *Journal of Traditional and Complementary Medicine 9*, 383-392. https://doi.org/10.1016/j.jtcme.2017.10.006

Bao, Y., Reddivari, L., and Huang, J.Y. (2020). Enhancement of phenolic compounds extraction from grape pomace by high voltage atmospheric cold plasma. *LWT 133*, 109970. https://doi.org/10.1016/j.lwt.2020.109970

Bonilla-Cruz, J., Lara-Ceniceros, T., Saldívar-Guerra, E., and Jiménez-Regalado, E. (2017). Towards controlled graft polymerization of poly[styrene- co-(maleic anhydride)] on functionalized silica mediated by oxoaminium bromide salt. Facile synthetic pathway using nitroxide chemistry. *Macromolecular Rapid Communications 28*, 1397-1403. https://doi.org/10.1002/marc.200700182

Campo Vera, Y., Delgado, M.A., Roa, Y., and Mora, G. (2017). Efecto antimicrobiano del quitosano y cascara de naranja en el tratamiento de aguas residuales. *Revista de Investigaciones Altoandinas 19*, 381-388. http://dx.doi.org/10.18271/ria.2017.312

Chytrosz-Wrobel, P., Golda-Cepa, M., Stodolak-Zych, E., Rysz, J., and Kotarba, A. (2023). Effect of oxygen plasma-treatment on surface functional groups, wettability, and nanotopography features of medically relevant polymers with various crystallinities. *Applied Surface Science Advances 18*, 100497. https://doi.org/10.1016/j.apsadv.2023.100497

Colín-Orozco, E. Síntesis de polímeros biocompatibles por plasma. Tesis de mestría Universidad Autónoma Metropolitana, Unidad Azcaportzalco.

Constante, C.K., Rodríguez, J., Sonnenholzner, S., and Domínguez-Borbor, C. (2022). Adaptation of the methyl thiazole tetrazolium (MTT) reduction assay to measure cell viability *in vibrio spp. Aquaculture 560*, 738568. https://doi.org/10.1016/j.aquaculture.2022.738568

Corazzari, I., Nisticò, R., Turci, F., Faga, M.G., Franzoso, F., Tabasso, S., and Magnacca, G. (2015). Advanced physico-chemical characterization of chitosan by means of TGA coupled on-line with FTIR and GCMS: Thermal degradation and water adsorption capacity. *Polymer Degradation and Stability 112*, 1-9. https://doi.org/10.1016/j.polymdegradstab.2014.12.006

Deng, P., Yao, L., Chen, J., Tang, Z., and Zhou, J. (2022). Chitosan-based hydrogels with injectable, self-healing, and antibacterial properties for wound healing. *Carbohydrate Polymers 276*, 118718. https://doi.org/10.1016/j.carbpol.2021.118718

Dong, Y., Yonghong, R., Huiwi, W., Zhao, Y., and Bi, D. (2004). Studies on glass transition temperature of chitosan with four techniques. *Journal of Applied Polymer Science 93*, 1553-1558. https://doi.org/10.1002/app.20630

Embuscado, M.E. (2015). Spices and herbs: Natural sources of antioxidants - a mini review. *Journal of Functional Foods 18*, 811-819. https://doi.org/10.1016/j.jff.2015.03.005

Feng, S., Liu, F., Guo, Y., Ye, M., He, J., Zhou, H., Liu, L., Cai, L., Zhang, Y., and Li, R. (2021). Exploring the role of chitosan in affecting the adhesive, rheological, and antimicrobial properties of carboxymethyl cellulose composite hydrogels. *International Journal of Biological Macromolecules 190*, 554-563. https://doi.org/10.1016/j.ijbiomac.2021.08.217

Fridman, A. (2008). *Plasma Chemistry*. Cambridge University Press, 1-1022.

Fridman, A. (2023). *Plasma Physics and Engineering*, 2023.

Ge, Y., Chen, X., Wang, X., Yuan, L., Wu, J., and Yao, J. (2022). Preparation, characterization and antibacterial activity evaluation of N-acetylneuraminic acid-crosslinked chitosan hydrogels. *Polymer Testing 106*, 107457. https://doi.org/10.1016/j.polymertesting.2021.107457

Guo, Y., Qu, Y., Yu, J., Song, L., Chen, S., Qin, Z., Gong, J., Zhan, H., Gao, Y., and Zhang J. (2022). A chitosan-vitamin C based injectable hydrogel improves cell survival under oxidative stress. *International Journal of Biological*

*Macromolecules 202*, 102-111. https://doi.org/10.1016/j.ijbiomac.2022.01.030

Hernández-Ochoa, L., Gonzales-Gonzales, A., Gutiérrez-Méndez, N., Muñoz-Castellanos, L.N., and Quintero Ramos, A. (2011). Estudio de la actividad antibacteriana de películas elaboradas con quitosano a diferentes pesos moleculares incorporando aceites esenciales y extractos de especias como agentes antimicrobianos. *Revista Mexicana de Ingeniería Química 10*, 455-463.

Huang, L., Wang, W., Xian, Y., Liu, L., Fan, J., Liu, H., Zheng, Z., and Wu, D. (2023). Rapidly *in situ* forming an injectable Chitosan/PEG hydrogel for intervertebral disc repair. *Materials Today Bio 22*, 100752. https://doi.org/10.1016/j.mtbio.2023.100752 Karadağ, A.E., Demirci, B., Çaşkurlua, A., Demirci, F., Okur, Y., Orak, D., Sipahi, H., and Base, K.H.C. (2019). In vitro antibacterial, antioxidant, anti-inflammatory, and analgesic evaluation of *Rosmarinus officinalis* L. flower extract fractions. *South African Journal of Botany 125*, 214-220. https://doi.org/10.1016/j.sajb.2019.07.039

Kumar, N., Mahade, S., Ganvir, A., and Joshi, S. (2021). Understanding the influence of microstructure on hot corrosion and erosion behavior of suspension plasma sprayed thermal barrier coatings. *Surface and Coatings Technology 419*, 127306. https://doi.org/10.1016/j.surfcoat.2021.127306

Levien, M., Amin, I., Vicente, F., Kodaira, P., and Weltmann, K.D. (2023). Direct grafting of microwrinkled hydrogels by atmospheric-pressure plasma polymerization: Going simple and environmentally friendly. *European Polymer Journal 198*, 112413. https://doi.org/10.1016/j.eurpolymj.2023.112413

Li Shan, T., Hui Li, T., Karthik, D., Yeon Yin, W., Saravanan, M., Kamaruddin, H., and Janarthanan, P. (2021). Fabrication of radiation cross-linked diclofenac sodium loaded carboxymethyl sago pulp/chitosan hydrogel for enteric and sustained drug delivery. *Carbohydrate Polymer Technologies and Applications 2*, 100084. https://doi.org/10.1016/j.carpta.2021.100084

Liu, F., Wang, L., Zhai, X., Ji, S., Ye, J., Zhu, Z., Teng, C., Dong, W., and Wei, W. (2023). A multi-functional double cross-linked chitosan hydrogel with tunable mechanical and antibacterial properties for skin wound dressing. *Carbohydrate Polymers 322*, 121344. https://doi.org/10.1016/j.carbpol.2023.121344

Madni, M., Kousar, R., Naeem, N., and Wahid, F. (2021). Recent advancements in applications of chitosan-based biomaterials for skin tissue engineering. *Journal of Bioresources and Bioproducts 6*, 11-25. https://doi.org/10.1016/j.jobab.2021.01.002

Maiz-Fernández, S., Guaresti, O., Perez, L., Ruiz-Rubio, L., Gabilondo, N., Vilas, J., and Lanceros-Méndez, S. (2020). $\beta$-glycerol phosphate/genipin chitosan hydrogels: A comparative study of their properties and diclofenac delivery. *Carbohydrate Polymers 248*, 116811. https://doi.org/10.1016/j.carbpol.2020.116811

Men, Y.L., Liu, P., Meng, X.Y., and Pan, X.Y. (2022). Recent progresses in material fabrication and modification by cold plasma technique. *FirePhysChem*, https://doi.org/10.1016/j.fpc.2022.01.001

Mena-Huertas, S.J., García-López, J.P., Nicola-Benavides, S.N., and Yépez-Chamorro, M.C. (2016). Inocuidad citotóxica y mutagénica de los aceites esenciales de *Rosmarinus officinalis* L. y *Ruta graveolens* L. promisorios para el tratamiento complementario de la infección por *Helicobacter pylori. Actualidades Biológicas 38*, 37-44. https://doi.org/10.17533/udea.acbi.v38n104a04

Navascués, P., Buchtelová, M., Zajícková, L., Rupper, P., and Hegemann, D. (2023). Polymerization mechanisms of hexamethyldisiloxane in low-pressure plasmas involving complex geometries. *Applied Surface Science*, 158824. https://doi.org/10.1016/j.apsusc.2023.158824

Niladri Sekhar, C., Hema Girija, S., Pavan Kumar, D., Balaraman, G., Muhamed, A., Rangasamy, A., Suseela, M., and Ravishankar Chandragiri, N. (2022). Nano-encapsulation of curcumin in fish collagen grafted succinyl chitosan hydrogel accelerates wound healing process in experimental rats. *Food Hydrocolloids for Health 2*, 100061. https://doi.org/10.1016/j.fhfh.2022.100061

Okyere, A.Y., Rajendran, S., and Annor, G.A. (2022). Cold plasma technologies: Their effect on starch properties and industrial scale-up for starch modification. *Current Research in Food Science 5*, 451-63. https://doi.org/10.1016/j.crfs.2022.02.007

Pérez-Huertas, S., Terpilowski, K., Tomczynska Mleko, M., and Mleko, S. (2024). Tailoring the surface and rheological properties of gelatine-based hydrogel films via indirect cold plasma treatment for engineering applications. *Journal of Food Engineering 363*, 260-8774. https://doi.org/10.1016/j.jfoodeng.2023.111781.

Reyna-Martínez, R., Narro Céspedes, R.I., Alonso Ibarra, M.C., and Reyes Acosta, Y. (2018). Use of cold plasma technology in biomaterials and their potential utilization in controlled administration of active substances. *Journal Material Science 4*.

Rezaei, F.S., Sharifianjazi, F., Esmaeilkhanian, A., and Salehi, E. (2021). Chitosan films and scaffolds for regenerative medicine applications: A review. *Carbohydrate Polymers 273*, 118631. https://doi.org/10.1016/j.carbpol.2021.118631

Rodríguez-Guzmán, C.A., Montaño-Leyva, B., Sánchez-Burgos, J.A., Bautista-Rosales, P.U., and Gutiérrez-Martínez, P. (2022). Chitosan and GRAS substances application in the control of *Geotrichum candidum* isolated from tomato fruits (*Lycopersicum esculentum L.*) in the state of Nayarit, Mexico: *in vitro* test. *Revista Mexicana de Ingeniería Química 21*, Bio2790. https://doi.org/10.24275/rmiq/BiO2790

Sadeghi, A., Razavi, S.M.A., and Shahrampour, D. (2022). Fabrication and characterization of biodegradable active films with modified morphology based on polycaprolactone-polylactic acid-green tea extract. *International Journal of Biological Macromolecules 205*, 341-356. https://doi.org/10.1016/j.ijbiomac.2022.02.070

Sanchez Armengol, E., Grassiri, B., Piras, A.M., Zambito, Y., Fabiano, A., and Laffleur, F. (2024). Ocular antibacterial chitosan-maleic acid hydrogels: *In vitro* and *in vivo* studies for a promising approach with enhanced mucoadhesion. *International Journal of Biological Macromolecules 254*, 127939. https://doi.org/10.1016/j.ijbiomac.2023.127939

Sánchez-Camargo, A., and Herrero M. (2017). Rosemary (*Rosmarinus officinalis*) as a functional ingredient: recent scientific evidence. *Current Opinion in Food Science 14*, 13-19. https://doi.org/10.1016/j.cofs.2016.12.003

Shrivastav, A., Gunawardena, A.M., Liu, D.S., Liu, Z., and Tam, H.Y. (2020). Microstructured optical fiber based Fabry-Pérot interferometer as a humidity sensor utilizing chitosan polymeric matrix for breath monitoring. *Scientific Reports 10*, 6002. https://doi.org/10.1038/s41598-020-62887-y

Singha, I., and Basu, A. (2022). Chitosan based injectable hydrogels for smart drug delivery applications. *Sensors International 3*, 100168. https://doi.org/10.1016/j.sintl.2022.100168

Sundriyal, P., Sahu, M., Prakash, O., and Bhattacharya, S. (2021). Long-term surface modification of PEEK polymer using plasma and PEG silane treatment. *Surfaces and Interfaces 25*, 101253. https://doi.org/10.1016/j.surfin.2021.101253

Tran, D.L., Le-Thi, P., Hoang, Thi, T.T., and Park, K.D. (2020). Novel enzymatically crosslinked chitosan hydrogels with free-radical-scavenging property and promoted cellular behaviors under hyperglycemia. *Progress in Natural Science: Materials International 30*, 661-668. https://doi.org/10.1016/j.pnsc.2020.08.004

Tzima, K., Brunton, N.P., Lyng, J., Frontuto, D., and Rai, D.K. (2021). The effect of Pulsed Electric field as a pre-treatment step in ultrasound assisted extraction of phenolic compounds from fresh rosemary and thyme by-products. *Innovative Food Science & Emerging Technologies 69*, 102644. https://doi.org/10.1016/j.ifset.2021.102644

Wiącek, A., Gozdecka, A., Jurak, M., Przykaza, K., and Terpiłowski, K. (2018). 45S5 Bioglass Composition 21.04% Si 17.5% Ca 18.2% Na 2.6%P 40. https://doi.org/10.1016/j.colsurfa.2018.04.061

Yan, X., Liu, Z., Diao, M., and Zhang, T. (2022). Effect of molecular weight of chitosan on properties of chitosan-Zn nanoparticles. *Food Bioscience 50*, 102206. https://doi.org/10.1016/j.fbio.2022.102206

Yuan, H., Li, W., Song, C., and Huang, R. (2022). An injectable supramolecular nanofiber-reinforced chitosan hydrogel with antibacterial and anti-inflammatory properties as potential carriers for drug delivery. *International Journal of Biological Macromolecules*. https://doi.org/10.1016/j.ijbiomac.2022.02.015

Zapata-Luna, R.L., Davidov-Pardo, G., Pacheco, N., and Ayora-Talavera, T., Espinosa-Andrews, H.,

García-Márquez, E., and Cuevas-Bernardino, J.C. (2023). Structural and physicochemical properties of bio-chemical chitosan and its performing in an active film with quercetin and *Phaseolus polyanthus* starch. *Revista Mexicana de Ingeniería Química 22*, Alim2315. https://doi.org/10.24275/rmiq/Alim2315

Zhengbo, L., Lei, Z., Xiaoman, Z., Di, H., and Yongjun, Z. (2022). High strength chitosan hydrogels prepared from NaOH/urea aqueous solutions: the role of thermal gelling. *Carbohydrate Polymers 297*, 120054. https://doi.org/10.1016/j.carbpol.2022.120054

Zhong, X., Wang, X., Zhou, N., Li, J., Liu, J., Yue, J., Hao, X., Gan, M., Lin, P., and Shang. X. (2020). Chemical characterization of the polar antibacterial fraction of the ethanol extract from *Rosmarinus officinalis*. *Food Chemistry 344*, 128674. https://doi.org/10.1016/j.foodchem.2020.128674

Zhu, D.Y., Chen, Z.P., Hong, Z.P., Zhang, L., Liang, X., Li, Y., Duan, X., Luo, H., Peng, J., and Guo, J. (2022). Injectable thermo-sensitive and wide-crack self-healing hydrogel loaded with antibacterial anti-inflammatory dipotassium glycyrrhizate for full-thickness skin wound repair. *Acta biomaterialia 143*, 203-215. https://doi.org/10.1016/j.actbio.2022.02.041

Zhu, Y., Zhang, J., Song, J., Yang, J., Du, Z., Zhao, W., Guo, H., Wen, C., Li, Q., Sui, X., and Zhang, L. (2020). A multifunctional pro-healing zwitterionic hydrogel for simultaneous optical monitoring of pH and glucose in diabetic wound treatment. *Advanced Functional Materials 30*, 1905493. https://doi.org/10.1002/adfm.201905493